THE JOURNAL OF BIOLOGICAL CHEMISTRY VOL. 289, NO. 21, pp. 14925–14940, May 23, 2014

Adducin Is Required for Desmosomal Cohesion in Keratinocytes*

Received for publication, October 18, 2013, and in revised form, March 31, 2014 Published, JBC Papers in Press, April 7, 2014, DOI 10.1074/jbc.M113.527127

Vera Rötzer[‡], Andreas Breit[§], Jens Waschke[‡1], and Volker Spindler[‡2]

From the [‡]Institute of Anatomy and Cell Biology, Ludwig-Maximilians-Universität, Munich D-80336 and the [§]Walther-Straub-Institute for Pharmacology and Toxicology, Ludwig-Maximilians-Universität, Munich D-80336, Germany

Background: The cortical actin cytoskeleton is necessary for keratinocyte adhesion by unclear mechanisms.
Results: The actin-binding protein adducin modulates desmosomal adhesion and is a target of protective PKC phosphorylation in response to autoantibodies of the blistering skin disease pemphigus.
Conclusion: Adducin promotes adhesion by regulating desmosomes and is part of a protective pathway in pemphigus.
Significance: Novel mechanism how cortical actin modulates desmosomal adhesion.

Adducin is a protein organizing the cortical actin cytoskeleton and a target of RhoA and PKC signaling. However, the role for intercellular cohesion is unknown. We found that adducin silencing induced disruption of the actin cytoskeleton, reduced intercellular adhesion of human keratinocytes, and decreased the levels of the desmosomal adhesion molecule desmoglein (Dsg)3 by reducing its membrane incorporation. Because loss of cell cohesion and Dsg3 depletion is observed in the autoantibody-mediated blistering skin disease pemphigus vulgaris (PV), we applied antibody fractions of PV patients. A rapid phosphorylation of adducin at serine 726 was detected in response to these autoantibodies. To mechanistically link autoantibody binding and adducin phosphorylation, we evaluated the role of several disease-relevant signaling molecules. Adducin phosphorylation at serine 726 was dependent on Ca^{2+} influx and PKC but occurred independent of p38 MAPK and PKA. Adducin phosphorylation is protective, because phosphorylation-deficient mutants resulted in loss of cell cohesion and Dsg3 fragmentation. Thus, PKC elicits both positive and negative effects on cell adhesion, since its contribution to cell dissociation in pemphigus is well established. We additionally evaluated the effect of RhoA on adducin phosphorylation because RhoA activation was shown to block pemphigus autoantibody-induced cell dissociation. Our data demonstrate that the protective effect of RhoA activation was dependent on the presence of adducin and its phosphorylation at serine 726. These experiments provide novel mechanisms for regulation of desmosomal adhesion by RhoA- and PKC-mediated adducin phosphorylation in keratinocytes.

Adducins are a family of actin-binding proteins comprised of three isoforms (α, β, and γ). The α- and γ-isoforms are ubiquitously expressed in most tissues, whereas β-adducin is most abundant in erythrocytes and brain (1). Adducin is the major component of the spectrin-based membrane cytoskeleton, thereby recruiting spectrin to actin filaments and promoting the assembly of a spectrin-actin meshwork underneath the plasma membrane (2, 3). Besides mediating the association between spectrin and F-actin, adducin is indispensable for the regulation of actin filaments via bundling and capping of the fast-growing end of actin filaments (4, 5). Moreover, it is well established that adducin localizes to cell-cell contacts *in vitro* (6) and *in vivo* (7) suggesting a relevance of adducin in proper assembly of F-actin bundles at intercellular junctions (8). The interaction of adducin with spectrin and actin is regulated by Ca^{2+} and calmodulin (4, 9) and through phosphorylation by various protein kinases such as protein kinase A (PKA), protein kinase C (PKC) (6, 10), and Rho-kinase (11, 12). It is noteworthy that Rho-GTPases are both important for actin cytoskeleton regulation (13–15) and are involved in signaling induced by autoantibodies in pemphigus (16–18).

Pemphigus vulgaris (PV)[3] is an autoimmune disease of the skin caused by autoantibodies directed against the adhesion molecules desmoglein (Dsg) 1 and 3 (19). There is growing evidence that both direct inhibition of Dsg3 interaction by antibody binding as well as intracellular signaling are necessary for intraepidermal blister formation (20). It has been shown that loss of keratinocyte cohesion in response to PV-IgG was accompanied by profound alterations of the cortical actin belt including fragmentation of actin filament bundles and increased stress fiber formation (21, 22). Pharmacological inhibition of p38 MAPK (21) or activation of RhoA (16–18) was sufficient to block the PV-IgG-mediated loss of cell adhesion as well as effects on actin cytoskeleton reorganization. Moreover, for RhoA-mediated protection against autoantibody-induced loss of cell cohesion a requirement of cortical actin polymeri-

* This work was supported by Deutsche Forschungsgemeinschaft Grant DFG SP1300-1 (to V. S.).
[1] To whom correspondence may be addressed: Pettenkoferstrasse 11, D-80336 Munich, Germany. Tel.: 49-89-2180-72610; Fax: 49-89-2180-72602; E-mail: jens.waschke@med.uni-muenchen.de.
[2] To whom correspondence may be addressed: Pettenkoferstrasse 11, D-80336 Munich, Germany. Tel.: 49-89-2180-72631; Fax: 49-89-2180-72602; E-mail: volker.spindler@med.uni-muenchen.de.

[3] The abbreviations used are: PV, pemphigus vulgaris; RhoA, Ras homolog gene family, member A; Dsg, desmoglein; DP, desmoplakin; CK, cytokeratin; CNF-1, cytotoxic necrotizing factor 1; CNFy, cytotoxic necrotizing factor y; Rac1, Ras-related C3 botulinum toxin substrate 1; Cdc42, cell division control protein 42 homolog; BIM-X, bisindolylmaleimide-X; BAPTA-AM, 1,2-bis(*o*-aminophenoxy)-ethane-*N*,*N*,*N*′,*N*′-tetraacetic acid; EEA-1, early endosomal antigen 1; FRAP, fluorescence recovery after photobleaching; HBSS, Hanks' buffered saline solution; n.t. siRNA, non-target siRNA; PMA, phorbol 12-myristate 13-acetate.

zation has been demonstrated (23). Concomitantly, a recent study reported a direct association of Dsg3 with actin and its involvement in actin dynamics (24).

In the first part of the present study, we focused on the role of adducin for desmosomal keratinocyte cohesion and on the turnover of Dsg3. Because we identified adducin to become phosphorylated in response to pemphigus autoantibodies, we tested the contribution of several known PV-relevant signaling molecules for adducin phosphorylation in the second part of the study.

EXPERIMENTAL PROCEDURES

Cell Culture and Test Reagents—The spontaneously immortalized human keratinocyte cell line HaCaT was grown in Dulbecco's modified Eagle's medium (Invitrogen) supplemented with 10% fetal bovine serum (Biochrom, Berlin, Germany), 50 units/ml of penicillin, and 50 μg/ml of streptomycin (both AppliChem, Darmstadt, Germany), and maintained in a humidified atmosphere containing 5% CO_2 at 37 °C. For all experiments 1×10^5 cells/cm^2 were seeded and grown in uncoated 24-well plates (Greiner Bio-One, Kremsmuenster, Austria) to confluence in high calcium medium (1.8 mM $CaCl_2x2H_2O$) within 4 days.

The PV serum was drawn from a patient with active PV suffering from both oral and skin lesions. The ELISA values (Euroimmun, Luebeck, Germany) were 11,550 (Dsg3) and 375 (Dsg1) units/ml. Purification of IgG was performed as described previously (22), and IgG fractions were applied at 0.5 mg/ml. AK23, a monoclonal pathogenic antibody derived from a pemphigus mouse model (25), was purchased from Biozol, Eching, Germany, and used at 75 μg/ml. A IgG fraction of a healthy volunteer was applied at 0.5 mg/ml. *Escherichia coli* cytotoxic necrotizing factor (CNF)-1 (activation of RhoA, Rac1 and Cdc42) and *Yersinia pseudotuberculosis* CNFy (activation of RhoA) were purchased from Cytoskeleton (Denver, CO) and preincubated at a dose of 1 mM for 6 h. Rho-kinase was effectively blocked by application of y27632 (Merck, Darmstadt, Germany) at a dose of 30 μM for 60 min. The p38 MAPK inhibitor SB202190 (Merck) was used at 30 μM for 30 min or 24 h, respectively. The PKC activator phorbol 12-myristate 13-acetate (PMA) (Sigma) was applied at 50 nM, the inhibitor BIM-X (Enzo Life Sciences, Loerrach, Germany) at 1 μM, and both were preincubated for 30 min. The PKA specific inhibitor H-89 (Sigma) was used at 10 μM and preincubated for 2 h. BAPTA-AM (Sigma), a cell-permeable Ca^{2+} chelator, was applied at 50 μM for 4 h.

Transfection—Adducin-specific small-interfering RNA (α-adducin siRNA: L-009487-00-0005 or γ-adducin siRNA: L-008468-00-0005) was purchased from Thermo Fisher Scientific/Dharmacon, Layfatte, IN. The plasmids pEGFP-C1-α-adducin, pEGFP-C1-α-adducin (S726A), pEGFP-C1-α-adducin (S716A/S726A), and pEGFP-C1-α-adducin (S726D) were kindly provided by Hong-Chen Chen (National Chung Hsing University, Taichung, Taiwan) (26). The plasmid pEGFP-N1-Dsg3 was a generous gift by Yasushi Hanakawa (Ehime University School of Medicine, Japan). For all experiments, HaCaT cells were cultured to 70–80% confluence in 24-well plates or in μ-slide 8-well imaging chambers (Ibidi, Martinsried, Germany) within 24 h and transfected with TurboFect^{TM} (Fermentas, Waltham, MA) according to the manufacturer's protocol. Cells were incubated with a final concentration of 0.78 μg/ml of siRNA for 24 h or 1.2 μg/μl of plasmid DNA for 8 h. Non-targeting (nt)-siRNA (Thermo Fisher Scientific/Dharmacon) or pEGFP-N1 served as controls. Fluorescent small interfering RNA was generated using the *Silencer*® siRNA Labeling Kit with Cy^{TM}3 dye (Invitrogen) in accordance with the manufacturer's instructions.

Immunofluorescence and Confocal Microscopy—HaCaTs were fixed for 10 min with 2% formalin (freshly prepared from paraformaldehyde) in PBS at room temperature. Monolayers were then treated with 0.1% Triton X-100 in PBS for 5 min and afterward blocked for 40 min with 10% normal goat serum and 1% BSA in PBS. Immunostaining was performed overnight at 4 °C with the following primary antibodies: α- and γ-adducin mAb (both Santa Cruz Biotechnology, Santa Cruz, CA), Dsg3 mAb (clone 5G11, Invitrogen), claudin-1 pAb (Invitrogen), E-cadherin (clone 36, BD Biosciences), Desmoplakin pAb (NW6, a kind gift of Kathleen Green, Northwestern University, Chicago, IL), EEA-1 pAb (ThermoFisher Scientific), and FITC-conjugated pan-cytokeratin mAb (Sigma). For visualization of F-actin, Alexa Fluor® 488 phalloidin (Invitrogen) was applied. As secondary antibodies Cy3- and Cy2-labeled goat anti-mouse or goat anti-rabbit Abs and a Cy5-conjugated goat anti-rabbit Ab were used (Dianova, Hamburg, Germany). Images were acquired using a Leica SP5 confocal microscope with a ×63 NA 1.4 PL APO objective (both Leica, Mannheim, Germany).

Fluorescence Recovery after Photobleaching (FRAP)—For FRAP studies, HaCaTs were seeded in 8-well imaging chambers and transfected with siRNA and plasmid DNA as described above. FRAP measurements were performed 48 h after transfection in a constant atmosphere at 37 °C with 5% CO_2 using an INU stage top incubator (Tokai Hit, Shizuoka-Ken, Japan). Using the FRAP wizard software (Leica), the GFP-Dsg3 signal was bleached after definition of regions of interests using the 488-nm laser line at 100% transmission and fluorescence recovery was captured over time. Fluorescence intensities were analyzed and normalized to the pre-bleach value using Excel (Microsoft, Redmond, WA).

Keratinocyte Dissociation Assay—Dispase-based dissociation assays were performed with fully confluent HaCaT monolayers in uncoated 24-well plates after transfection or treatment with the indicated conditions as described above. In general, cells were washed with Hanks' buffered saline solution (HBSS) and incubated with 150 μl of Dispase II (>2.4 units/ml in HBSS; both Sigma) for 20 min at 37 °C to detach the monolayer from the well bottom. Dispase solution was carefully replaced by 200 μl of HBSS and the cell monolayer was then mechanically stressed by pipetting up and down 7 times using a 1-ml electric pipette (Eppendorf, Hamburg, Germany). The resulting fragments were analyzed with a binocular microscope (Leica) at strictly the same magnification (field of view adjusted to cover the entire well). Every fragment that was visible was counted by the same researcher, who was blinded for the experimental condition of each well. Each independent experiment was carried out in duplicates or triplicates. In total, at least four independent experiments ($N \geq 4$) were performed for each

condition. (Throughout this study, *N* is used to indicate independent experiments, and *n* is used to indicate repetitions.)

RNA Isolation, cDNA Synthesis, and Standard Polymerase Reaction (PCR)—Total RNA of HaCaT cells was isolated using the RNeasy® Plus Mini Kit (Qiagen) according to the manufacturer's instructions. Subsequently, 1–4 μg of total RNA was reverse transcribed into first strand cDNA using SuperScript® II Reverse Transcriptase (Invitrogen). PCR was performed with 1 μg of cDNA using GoTaq® DNA Polymerase (Promega) in a C1000™ Thermal Cycler (Bio-Rad Laboratories). The PCR program comprised an initial denaturation step at 94 °C for 2 min followed by 30 cycles at 94 °C for 30 s and 55 °C for 30 s and a final extension for 7 min at 72 °C. PCR amplicons were visualized in ethidium bromide-stained agarose gels. The following primers were used: POLR2L (NM_021128.4) forward, 5′-CGAGTACACCGAGGGGA-3′ and reverse, 5′-GGTTTCAG-CGTGGTCACTT-3′; primer sequences for α- and γ-adducin were derived from Ref. 8.

Protein Extraction and Western Blotting—Protein extraction, Triton X-100 protein fractionation, and Western blot analysis were carried out as described previously (27). Briefly, cells were scraped in SDS-lysis buffer (containing 25 mmol/liter of HEPES, 2 mmol/liter of EDTA, 25 mmol/liter of NaF and 1% SDS) supplemented with protease-inhibitor mixture (Roche Applied Science). For protein fractionation, cells were incubated with Triton buffer (containing 0.5% Triton X-100, 50 mmol/liter of MES, 25 mmol/liter of EGTA, and 5 mmol/liter of $MgCl_2$) for 15 min on ice under gentle shaking. The whole protein pool was separated into a cytoskeletal (Triton-insoluble, pellet) and a non-cytoskeletal (Triton-soluble, supernatant) fraction by centrifugation for 5 min at 13,000 × *g*. After resuspending the pellet in SDS-lysis buffer, samples were sonificated and the protein concentration of each sample was measured using the BCA protein assay kit (Pierce/Thermo Scientific). Lysates were then subjected to gel electrophoreses and blots were probed with the following primary antibodies: Desmoplakin mAb (Epitomics, Burlingame, CA), α-tubulin mAb (Abcam), GAPDH mAb (Santa Cruz Biotechnologies), p38 MAPK pAb, phospho-p38 MAPK pAb (both Cell Signaling), phospho-S726-adducin pAb, α- and γ-adducin mAb, Dsg3 pAb (clone H-145), phospho-ERK mAb (Santa Cruz Biotechnologies), and ERK1/2 pAb (Cell Signaling). For protein detection polyclonal HRP-conjugated goat anti-rabbit (Cell Signaling) or goat anti-mouse (Dianova) IgG Abs and an ECL reaction system (self-made solutions) were used.

Aequorin Luminescence-based Calcium Assay—Intracellular Ca^{2+} levels in response to stimuli were quantified using the Ca^{2+}-sensitive aequorin-eGFP fusion protein (pEGFP-C1-G5α) previously reported (28). HaCaTs were seeded in 96-well microplates (PerkinElmer Life Sciences), transfected with the pEGFP-C1-G5α plasmid, and analyzed 48 h post-transfection in a plate reader (FLUOstar® Omega, BMG Labtech, Ortenburg, Germany) at 37 °C. After labeling the cells with coelenterazin H (5 μM, Biaffin, Kassel, Germany) in HBSS, HBSS alone, or HBSS including PV-IgG or control IgG was automatically injected 20 s after starting the measurement. Total emission (λ_{max}, 509 nm) was measured in 2-s intervals.

Rac and Rho Protein Activation Assay—To test the pharmacological activators CNF-1 or CNFy and the effects of AK23 or PV-IgG on activation of Rac and RhoA, HaCaTs were grown on 24-well plates and treated with the respective substances before being subjected to G-LISA® Rac or RhoA activity assays (Cytoskeleton). Assays were applied following the manufacturer's protocol and the optical density was read with a plate reader device at 490 nm (TECAN, Maennedorf, Switzerland).

Image Analyses—The intensity of cortical actin was evaluated in ImageJ as arbitrary units by drawing a rectangle with a fixed size over the membrane in each quadrant of a cell double labeled for F-actin and α- or γ-adducin and background intensity measured on an uncovered area of the slide was subtracted. Then the four intensity values obtained per cell and color were averaged and plotted as dot plot with the *x* axis representing α- or γ-adducin and F-actin shown on the *y* axis. Thus, each data point represents a single cell.

The fragmentation index was calculated by measuring the length of the cell circumference and the length of the cortical F-actin underneath the membrane. F-actin length was divided by the length of the cell circumference, yielding the percentage of the membrane that was covered by F-actin in a given cell. Analysis was carried out in cells transfected with n.t.-siRNA and cells were transfected with either α- or γ-adducin siRNA. In the latter two cases, we also distinguished between cells with clear knockdown and cells without effective knockdown. This was possible because these two cell populations were clearly distinguishable in the respective adducin staining.

The width of Dsg3 staining on the membrane was quantified by measuring the length of Dsg3 perpendicular to the cell membrane in each quadrant of a cell. The resulting values were averaged yielding a mean value of Dsg3 width per cell.

Statistics—Error bars represent mean ± S.E. Data for two groups were compared using two-tailed Student's *t* test. For multiple group comparisons, analysis of variance was performed followed by Bonferroni post hoc test. Statistical significance was assumed when $p < 0.05$.

RESULTS

Adducin Silencing Promoted Cell Dissociation and Reduced Desmosmal Dsg3 Protein Content—In fully confluent HaCaT, both α- and γ-adducin were expressed in comparable amounts as detected on mRNA (Fig. 1, *A* and *B*) and protein level (Fig. 1*C*) and colocalized extensively with the cortical actin belt (Fig. 1*D*). Under conditions of effective silencing via siRNA (Fig. 1, *B* and *C*), both adducin isoforms were absent in large areas of the monolayer (Fig. 1*D*). In these areas, the cortical actin belt appeared strongly disorganized and fragmented (*arrows*) compared with cells unaffected by siRNA transfection. This is also reflected in the image analysis by which the cortical F-actin intensity was reduced under conditions of decreased adducin staining intensity (Fig. 1*E*). Here, each data point represents a single cell, the *blue* colored points denote cells with clearly positive knockdown, the *purple* spots are cells in which apparently the knockdown was not effective. The F-actin intensity in cells with visible knockdown was significantly reduced in comparison to non-target controls or cells unaffected by adducin targeting. An evaluation of cortical actin fragmentation was car-

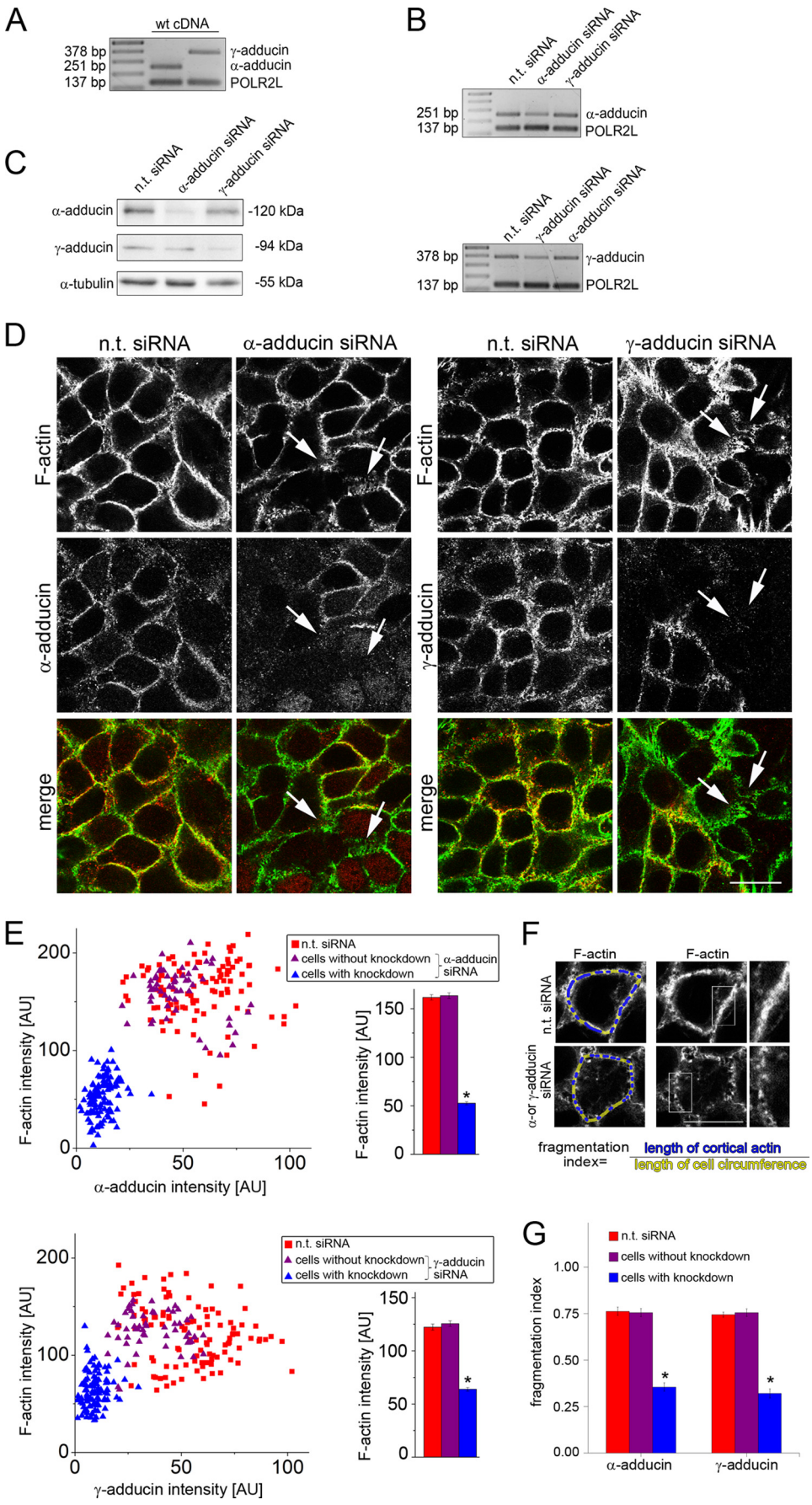
A
wt cDNA
378 bp
251 bp
137 bp
γ-adducin
α-adducin
POLR2L
B
n.t. siRNA
α-adducin siRNA
γ-adducin siRNA
251 bp
137 bp
α-adducin
POLR2L
n.t. siRNA
γ-adducin siRNA
α-adducin siRNA
378 bp
137 bp
γ-adducin
POLR2L
C
n.t. siRNA
α-adducin siRNA
γ-adducin siRNA
α-adducin
γ-adducin
α-tubulin
-120 kDa
-94 kDa
-55 kDa
D
n.t. siRNA
α-adducin siRNA
n.t. siRNA
γ-adducin siRNA
F-actin
α-adducin
γ-adducin
merge
E
n.t. siRNA
cells without knockdown
cells with knockdown
α-adducin siRNA
F-actin intensity [AU]
α-adducin intensity [AU]
γ-adducin siRNA
γ-adducin intensity [AU]
F
F-actin
n.t. siRNA
α-or γ-adducin siRNA
fragmentation index=
length of cortical actin
length of cell circumference
G
n.t. siRNA
cells without knockdown
cells with knockdown
fragmentation index
α-adducin
γ-adducin

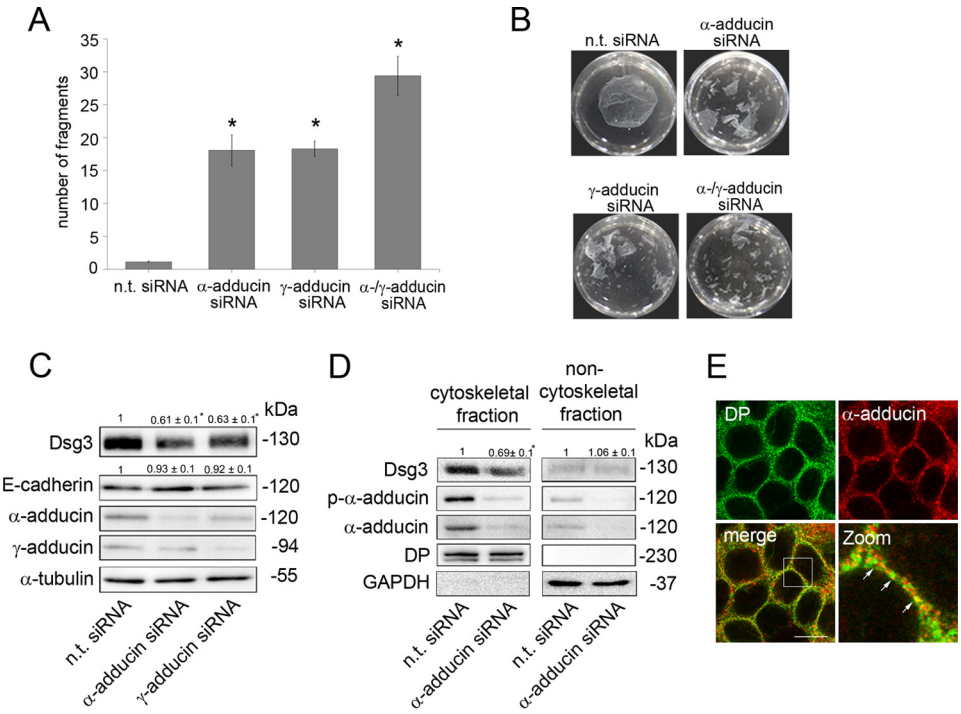

FIGURE 2. **Adducin silencing promotes cell dissociation and reduces desmosomal Dsg3 levels.** *A,* after siRNA-mediated silencing of the respective adducin isoform, confluent monolayers were subjected to dispase-based dissociation assays. Specific adducin knockdown resulted in a significant increase of fragment numbers compared with controls and silencing of both adducin isoforms led to further loss of cell adhesion ($N = 7$, $n > 14$, *, $p < 0.05$ *versus* control). *B,* representative images of monolayer fragmentation that were taken immediately after assay performance. *C,* immunoblot analysis demonstrated a decrease of Dsg3 but not of E-Cadherin protein levels after isoform-specific knockdown of adducin ($N = 5$, *, $p < 0.05$ *versus* control). *D,* Triton X-100 separation of cell lysates displayed a specific depletion of Dsg3 in the cytoskeleton-associated fraction after adducin knockdown. DP was used to indicate the desmosomal pool and GAPDH served as a marker of the non-cytoskeleton-bound fraction ($N = 5$, *, $p < 0.05$). *E,* partial colocalization of DP and α-adducin (*arrows*) ($N = 3$).

ried out as described in Fig. 1*F*. Indeed, the length of cortical actin was significantly reduced in cells displaying α- or γ-adducin silencing but not in cells unaffected by the knockdown or transfected with non-targeting siRNA (fragmentation index for α-adducin: 0.36 ± 0.02 (knockdown) *versus* 0.76 ± 0.02 (without transfection) and 0.76 ± 0.03 (n.t. siRNA); fragmentation index for γ-adducin: 0.32 ± 0.01 (knockdown) *versus* 0.75 ± 0.03 (without transfection) and 0.74 ± 0.02 (n.t.-siRNA) (Fig. 1*G*).

We next measured cell cohesion of HaCaT keratinocytes after adducin knockdown using dispase-based dissociation assays. Control knockdown cells were largely resistant to mechanical stress (fragment numbers: 1.1 ± 0.1), whereas silencing of either α- or γ-adducin increased fragment numbers to 18.1 ± 2.4 and 18.3 ± 1.4, respectively (Fig. 2, *A* and *B*). Silencing of both α- and γ-adducin led to a further increase of cell dissociation (29.4 ± 2.9 fragments).

Previously, adducins were demonstrated to be involved in adherens and tight junction remodeling in SK-CO15 cells (8). Because our studies demonstrated loss of cell adhesion following adducin silencing, we investigated the expression of desmosmal and adherens junction molecules. After gene silencing of either adducin isoform, the amount of Dsg3, a desmosomal adhesion molecule highly relevant for keratinocyte cell adhesion (27), was significantly decreased to 60.5 ± 8.9 (α-adducin knockdown) or 63.1 ± 5.1% (γ-adducin knockdown) compared with controls (Fig. 2*C*). This effect seemed to be restricted to desmosomes, as the adherens junction molecule E-cadherin was not significantly affected by adducin silencing (E-cadherin protein level: 93.2 ± 6.1 and 92.1 ± 8.2%, respectively). Because the effects of silencing of either α- or γ-adducin were identical, we further focused on α-adducin only. To examine whether Dsg3 was depleted from desmosomes or from non-cytoskeleton-associated pools, we performed Triton X-100 extraction of HaCaT lysates after α-adducin knockdown. In contrast to the non-cytoskeleton-bound fraction (105.8 ± 5.6%), a decrease of Dsg3 levels to 69.0 ± 8.7% of controls was detectable in the cytoskeleton-associated fraction (Fig. 2*D*). Desmoplakin (DP) served as marker for the desmosomal pool, GAPDH indicated the non-cytoskeletal fraction. Interestingly, a partial colocalization of adducin with DP was visible by immunostaining (Fig. 2*E*, *arrows*).

FIGURE 1. **siRNA-mediated depletion of α- and γ-adducin results in cortical actin fragmentation in HaCaT cells.** *A*, representative PCR analysis of α- and γ- adducin expression and *B,* detection of specific knockdown of either adducin isoforms, 4 independent experiments ($N = 4$). *C,* in Western blot analysis, both adducin isoforms were detectable after control knockdown (*n.t. siRNA*). Compared with controls, the most effective decrease of adducin protein levels were achieved after 72 h of siRNA gene silencing ($N = 4$). *D*, after immunostaining, in cells with efficient α- or γ-adducin silencing, the cortical actin belt appeared strongly disorganized in areas without adducin expression (*arrows*). *Scale bar*: 20 μm ($N = 4$). *E,* analysis showed a decrease of cortical F-actin intensity in cells with effective adducin silencing (*blue triangles*) compared with cells unaffected by adducin siRNA (*purple triangles*) or with control knockdown (*red squares*). Each data point represents a single cell. Graphs on the *right* denote the mean F-actin intensity of these three pools of cells. ($N = 3$, $n = 53–111$; *, $p < 0.05$ *versus* n.t. siRNA). *AU*, arbitrary units. *F,* schematic of the evaluation method of cortical actin fragmentation in control and siRNA-treated cells. *Scale bar*, 20 μm. *G,* length of cortical actin was significantly reduced in cells with α- or γ-adducin silenced HaCaTs compared with cells unaffected by knockdown or transfected with n.t.-siRNA (evaluation is based on $N = 3$, $n = 24$ cells, *, $p < 0.05$ *versus* control).

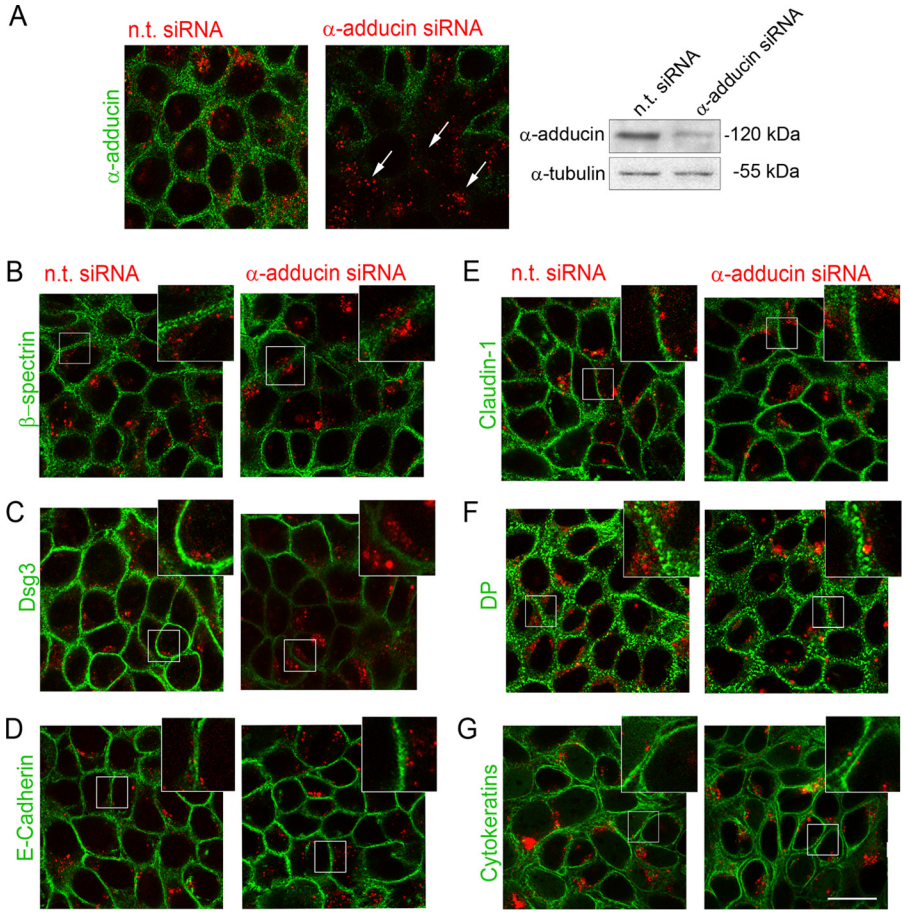

FIGURE 3. **Knockdown of α-adducin affects Dsg3 and β-spectrin distribution in HaCaTs.** *A,* for immunolocalization studies Cy3-labeled siRNA (*red*) was used. Effective α-adducin silencing was proven by immunostaining against α-adducin (*green*, *arrows*; *left two panels*) and in parallel by Western blot analysis (*right panel*). *B,* in cells with effective α-adducin knockdown, a reduction of β-spectrin staining was detectable. *C,* compared with control knockdown, cells with effective adducin silencing displayed reduced and diffusely distributed Dsg3 staining, whereas the localization of E-cadherin (*D*) and the tight junction molecule claudin-1 (*E*) was unaffected. Similarly, no changes in distribution of the desmosomal plaque protein DP or intermediate filament system (marked by a pan-cytokeratin antibody) were detectable in α-adducin siRNA-transfected cells (*F* and *G*). *Insets,* ×2.5 magnification of areas indicated. *Scale bar*, 20 μm, $N = 4$.

The effects of α-adducin silencing on adhesion molecules were also reproduced by immunolocalization studies. To indicate cells with effective knockdown, α-adducin siRNA was labeled (Fig. 3*A*, *arrows*). α-Adducin knockdown was also paralleled by reduction of β-spectrin, a known binding partner of adducins (Fig. 3*B*). Dsg3 staining appeared reduced in intensity and was more diffusely distributed at the cell membrane in cells with effective α-adducin siRNA uptake (Fig. 3*B*). However, in line with the Western blot experiments, this effect was not observed for E-cadherin localization (Fig. 3*C*). Similarly, the tight junction molecule claudin-1 was unaffected (Fig. 3*D*). DP tethers keratin filaments to other members of the desmosomal complex. We therefore investigated the distribution of DP (Fig. 3*F*) and cytokeratins (Fig. 3*G*) in cells with α-adducin silencing. However, no differences were detected compared with controls. Taken together, these results indicate that adducin is essential for keratinocyte cell-cell cohesion and is involved in the regulation of Dsg3 protein levels in desmosomes.

α-Adducin Silencing Delays Membrane Incorporation of Dsg3—Our data indicate that α-adducin regulates the turnover of Dsg3 in keratinocytes. We thus sought to investigate by which mechanisms adducin regulates Dsg3 content. We first tested whether α-adducin silencing promoted the internalization of Dsg3. However, colocalization of Dsg3 with the early endosome marker EEA-1 was a rather rare event under control knockdown conditions and was not increased after α-adducin silencing (Fig. 4, *A* and *B*, *arrows*). Therefore, we tested the other possibility that adducin is involved in membrane incorporation of Dsg3 and/or lateral mobility in the membrane, the latter of which may be necessary for incorporation into desmosomes (29). To test this hypothesis, we utilized FRAP. HaCaT cells were transfected with GFP-Dsg3 and either α-adducin or non-target siRNA (Fig. 4*C*). Interestingly, in α-adducin knockdown cells GFP-Dsg3 intensity at the membrane was reduced compared with controls (Fig. 4*D*). Furthermore, fluorescence recovery of GFP-Dsg3 in areas that were bleached by high power laser excitation was significantly reduced in cells with α-adducin silencing over the time of measurement (Fig. 4, *E* and *F*). These data suggest that adducin primarily regulates Dsg3 membrane incorporation and/or lateral mobility.

Pemphigus Autoantibodies and RhoA Induce Rapid Phosphorylation of Adducin—Given our finding that adducin silencing led to depletion of Dsg3, an event also elicited by application of pemphigus autoantibodies, we investigated the effects of an IgG fraction of PV patients (PV-IgG) on adducin localization. Incubation with PV-IgG for 24 h resulted in fragmentation of addu-

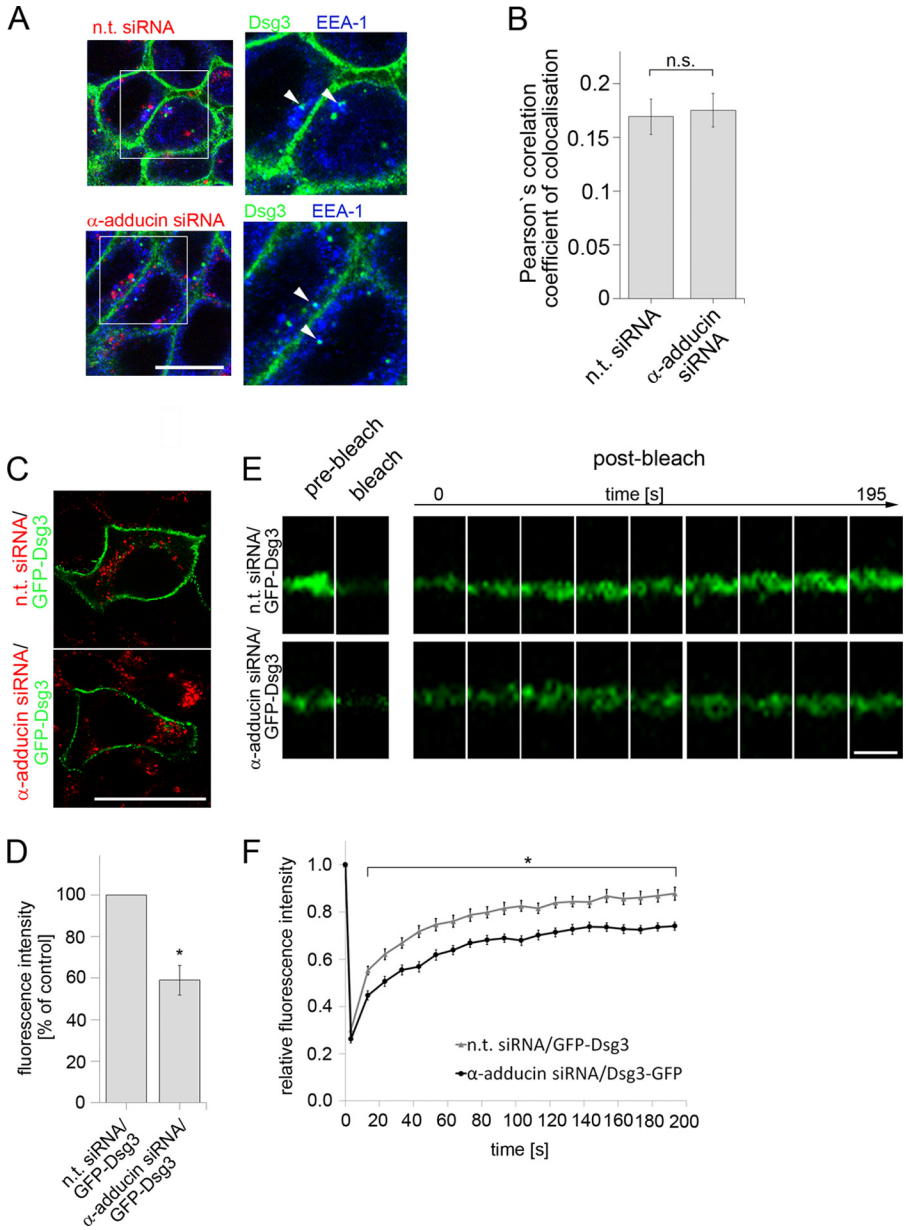

FIGURE 4. **Adducin regulates Dsg3 membrane incorporation.** *A*, immunofluorescence studies showed no alteration of colocalization of Dsg3 (*green*) and the early endosome marker (*EEA-1*, *blue*) (*arrows*) in cells transfected with α-adducin siRNA (*red*) compared with control knockdown cells. *Insets*, ×1.8 magnification of the indicated areas. *Scale bar*: 20 μm ($N = 4$). *B*, calculation of Pearson's correlation coefficient of colocalization of Dsg3 and EEA-1 ($N = 4$, $n > 21$). *C*, for FRAP analyses, HaCaTs were transfected with GFP-Dsg3 and either Cy3-labeled α-adducin siRNA or n.t.-siRNA. *Scale bar*: 20 μm. *D*, GFP-Dsg3 signal was reduced in cells with α-adducin silencing compared with controls. *E* and *F*, intensity measurement after photobleaching displayed reduced fluorescence recovery of GFP-Dsg3 in cells with α-adducin knockdown compared with controls (for all FRAP studies: $N = 3$, $n = 15$ cells, in each cell ≥5 regions of interests were analyzed, *, $p < 0.05$ *versus* control; *scale bar*, 2.5 μm).

cin staining at the membrane (Fig. 5*A*). This phenomenon was observed primarily at sites where intercellular gaps formed (*arrows*). Nevertheless, actin colocalization was preserved. Next, we analyzed adducin phosphorylation and protein levels in response to pemphigus autoantibodies. We applied PV-IgG (Fig. 5*B*, *middle panel*), or AK23, a pathogenic monoclonal antibody derived from a pemphigus mouse model (Fig. 5*B*, *lower panel*) to confluent HaCaT cells at time points ranging from 5 min to 24 h. No changes in α-adducin levels were detectable throughout this time frame (Fig. 5*B*). However, compared with incubation with control-IgG (Fig. 5*B*, *upper panel*), phosphorylation at Ser-726 was significantly increased after 10 min of PV-IgG incubation to 171.2 ± 11.9% and after AK23 incubation to 184.6 ± 16.7%. Similar effects were obtained for γ-adducin (data not shown). Collectively, these data demonstrate rapid adducin phosphorylation in response to pemphigus autoantibodies.

To investigate the mechanisms by which pemphigus autoantibodies lead to phosphorylation of adducin, we tested several pathways that are known to be altered in pemphigus. We here focused on RhoA, p38 MAPK, and PKC and PKA signaling.

The Protective Effect of Rho-GTPase Activation on Autoantibody-mediated Loss of Cell Cohesion Is Dependent on Adducin

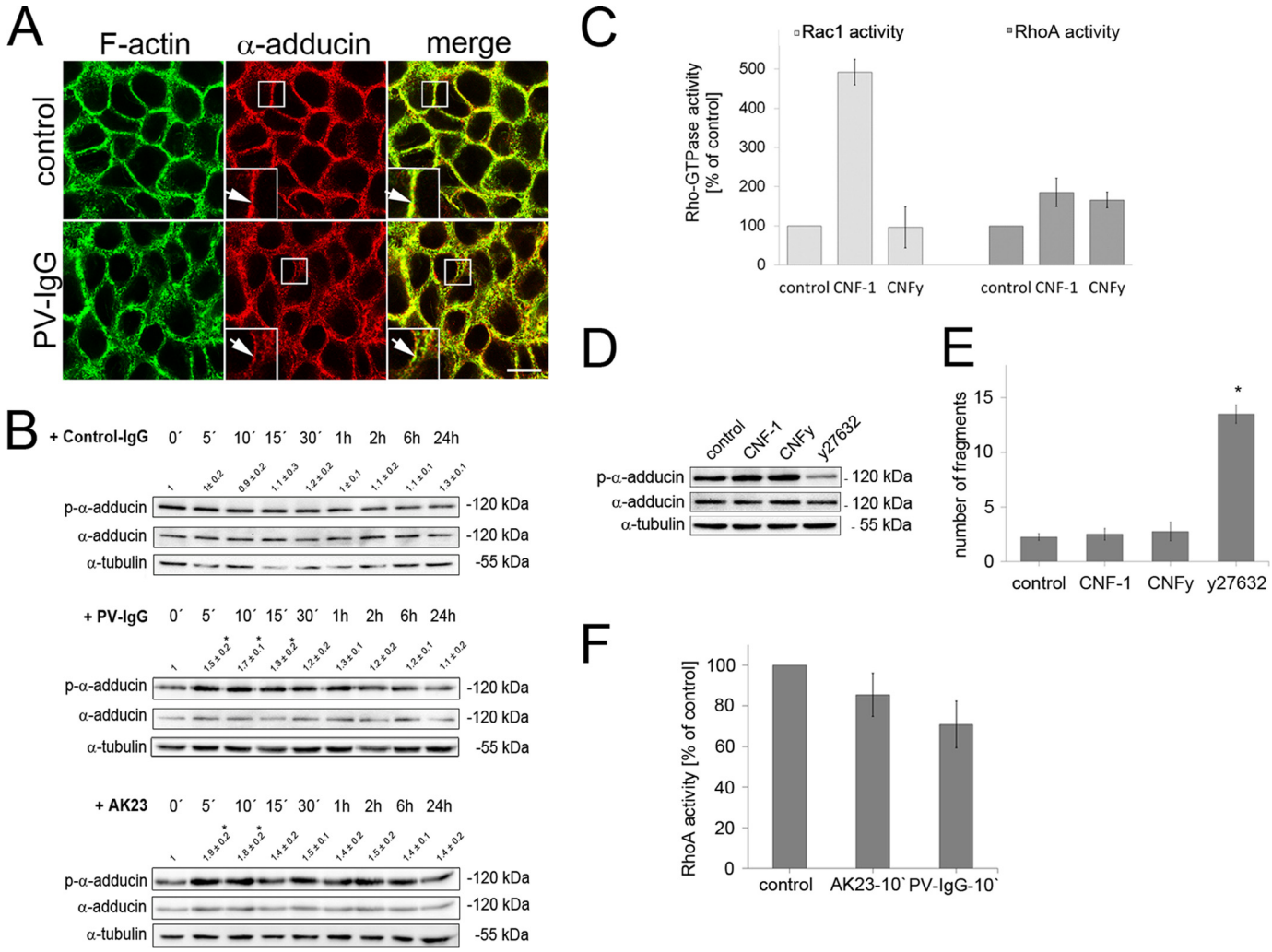

FIGURE 5. **Both pemphigus autoantibodies and RhoA phosphorylate adducin.** *A*, PV-IgG treatment for 24 h led to pronounced disorganization of F-actin (*green*) and α-adducin (*red*) (*arrows*). Insets: ×2 magnification of areas indicated. *Scale bar*, 20 μm ($N = 5$). *B*, incubation of PV-IgG or AK23 resulted in adducin phosphorylation at Ser-726. Time series analysis demonstrated an increased phosphorylation level starting after 5 to 10 min, whereas control IgG had no effect. Relative band intensity (*p-α-adducin/α-adducin*) as determined by densitometry is indicated *above each line*. Throughout this time frame no alterations in α-adducin levels were detectable ($N = 4$, *, $p < 0.05$ *versus* control). *C*, the specificity of CNF-1 (activation of RhoA, Rac-1, and CdC42) and CNFy (activation of RhoA) was tested by ELISA-based assays ($N = 3$). *D*, in Western blot analysis, incubation of CNF-1 or CNFy for 10 min caused profound adducin phosphorylation. Adversely, incubation with the specific Rho-kinase inhibitor y27632 for 1 h reduced adducin phosphorylation. *E*, in dissociation assays, incubation of CNF-1 or CNFy had no effect, whereas y27632 significantly increased the number of fragments compared with controls ($N = 6$, *, $p < 0.05$ *versus* control). *F*, ELISA-based assays displayed that incubation of PV-IgG or AK23 for 10 min reduced the activity of RhoA ($N = 3$).

Phosphorylation—Because previous data demonstrated that pharmacological activation of Rho-GTPases blocked PV-IgG-induced loss of cell adhesion and fragmentation of cortical actin (16, 17, 23), we first investigated the effects of the bacterial toxins CNF-1 (activation of RhoA, Rac1, and Cdc42) and CNFy (activation of RhoA) on phosphorylation of adducin. After testing the specificity of CNF-1 and CNFy in keratinocytes by ELISA-based assays (Fig. 5*C*), we treated HaCaTs with the respective compound. Interestingly, similar to AK23 and PV-IgG, both specific activation of RhoA by CNFy and activation of RhoA, Rac1, and Cdc42 by CNF-1 for 10 min (after preincubation for 6 h) led to adducin phosphorylation (Fig. 5*D*). Based on these data, we concluded that RhoA is the primary Rho family GTPase inducing adducin phosphorylation. In line with this, incubation of the Rho-kinase inhibitor y27632 for 1 h decreased the phosphorylation level below controls. Dispase-based assays revealed an increased number of fragments after y27632 incubation for 1 h (13.5 ± 0.8) but no alterations of cell cohesion by treatment with CNF-1 or CNFy alone (Fig. 5*E*). Because CNFy and CNF-1 had the same effect on adducin phosphorylation as pemphigus autoantibodies after 10 min, we tested whether these autoantibodies increase RhoA activity. However, RhoA activity was not elevated but rather reduced after 10 min (Fig. 5*F*), which is in line with previous data where RhoA levels were decreased after 24 h of PV-IgG incubation (16). Thus, adducin phosphorylation in response to PV-IgG incubation is independent of RhoA.

Next, we used CNFy under conditions of α-adducin silencing (Fig. 6*A*). In line with our previous studies, activation of Rho-GTPases was protective in control knockdowns as the AK23-induced increase of fragment numbers (20.5 ± 1.8) was blocked by co-incubation of CNFy (9.5 ± 1.0) and did not significantly differ from controls after 24 h (Fig. 6*B*). AK23 treatment for 24 h under conditions of α-adducin silencing further increased frag-

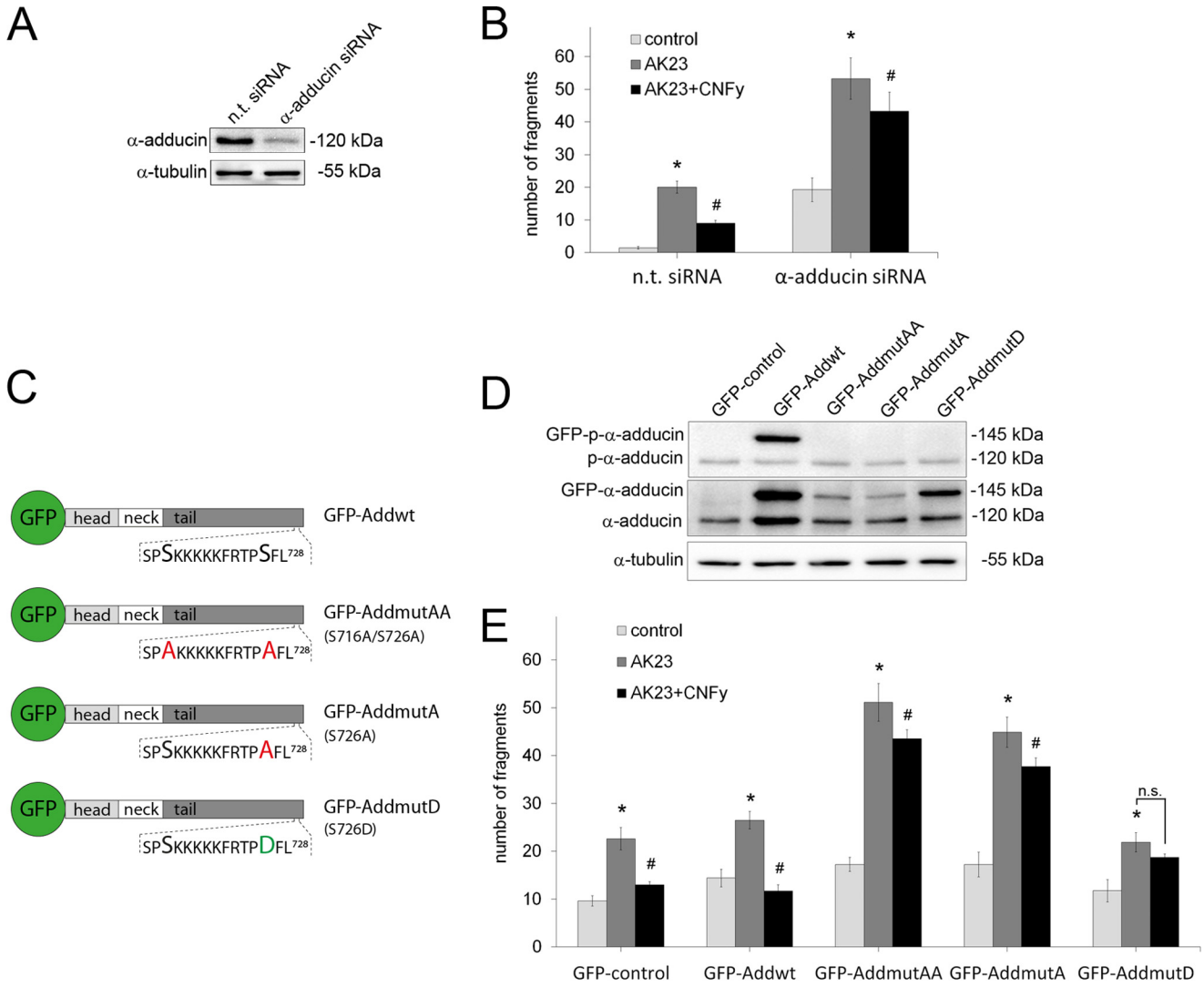

FIGURE 6. **The protective effect of Rho-GTPase activation is dependent on both adducin expression and phosphorylation at Ser-726.** *A*, representative Western blot of α- or γ-adducin silencing performed in parallel to dispase-based dissociation assays. *B*, in dissociation studies, AK23-induced loss of cell-cell adhesion after 24 h was significantly blocked in control knockdowns by co-incubation of CNFy. Under conditions of α- or γ-adducin silencing, AK23 incubation further increased the number of fragments. In these cells, AK23 effects were not significantly blocked by co-incubation with CNFy ($N = 5$, $n > 10$, *, $p < 0.05$ *versus* control; #, $p < 0.05$ *versus* AK23). *C*, schematic diagram of the constructs applied: GFP-α-adducin wild type (GFP-Addwt), GFP-α-adducin-S716A/S726A (GFP-AddmutAA), GFP-α-adducin-S726A (GFP-AddmutA), and GFP-α-adducin-S726D (GFP-AddmutD); and *D*, detection of efficient transfection by Western blot analysis. *E*, in dissociation assays, overexpression of GFP-Addwt resulted in similar fragment numbers as GFP-controls following 24 h of AK23 incubation. AK23-mediated loss of cell adhesion was significantly blocked in these cells. In contrast, AK23-induced fragmentation was drastically increased in cells expressing GFP-AddmutAA or GFP-AddmutA compared with GFP-Addwt cells and co-treatment with CNFy was only partially protective under these conditions. Also in GFP-AddmutD-transfected cells no protective effect was observed by CNFy, indicating that this mutant had no phosphomimetic activity under these conditions ($N = 6$, $n > 12$, *, $p < 0.05$ *versus* control; #, $p < 0.05$ *versus* AK23).

ment numbers (53.3 ± 6.3) compared with siRNA control. Importantly, under knockdown conditions AK23-mediated loss of cell cohesion was only partially blocked by CNFy co-incubation (fragment numbers: 43.25 ± 3.1, respectively) and still significantly differed to the respective control. Based on the finding that RhoA activation led to phosphorylation of α-adducin at Ser-726, we next applied several phospho mutants to test whether this modulates the protective effect of RhoA activation (Fig. 6*C*): GFP-α-adducin wild type (GFP-Addwt), GFP-α-adducin-S716A/S726A (GFP-AddmutAA), an α-adducin construct containing point mutations at Ser-716 and Ser-726 for alanine, GFP-α-adducin-S726A (GFP-AddmutA) with alanine mutation of Ser-726 only, and the phosphomimetic mutant GFP-α-adducin-S726D (GFP-AddmutD), in which Ser-726 was mutated to aspartic acid. Western blotting confirmed efficient transfection and demonstrated all GFP-Addmut constructs to be phosphorylation-deficient (Fig. 6*D*). Overexpression of GFP-Addwt yielded similar fragment numbers as GFP controls in dissociation assays following 24 h of AK23 incubation (26.5 ± 1.8 *versus* 22.6 ± 1.9) (Fig. 6*E*). Co-incubation with CNFy significantly blocked AK23-mediated loss of cell adhesion. Transfection of any of the GFP-Addmut constructs alone had no effect on fragment numbers under control conditions. Nevertheless, AK23-induced fragmentation was markedly increased in monolayers expressing GFP-AddmutAA and GFP-AddmutA compared with GFP-Addwt-transfected cells (51.1 ± 3.9 and 44.9 ± 3.1 *versus* 26.5 ± 1.8). Furthermore, under these conditions and similar to the results of α-adducin

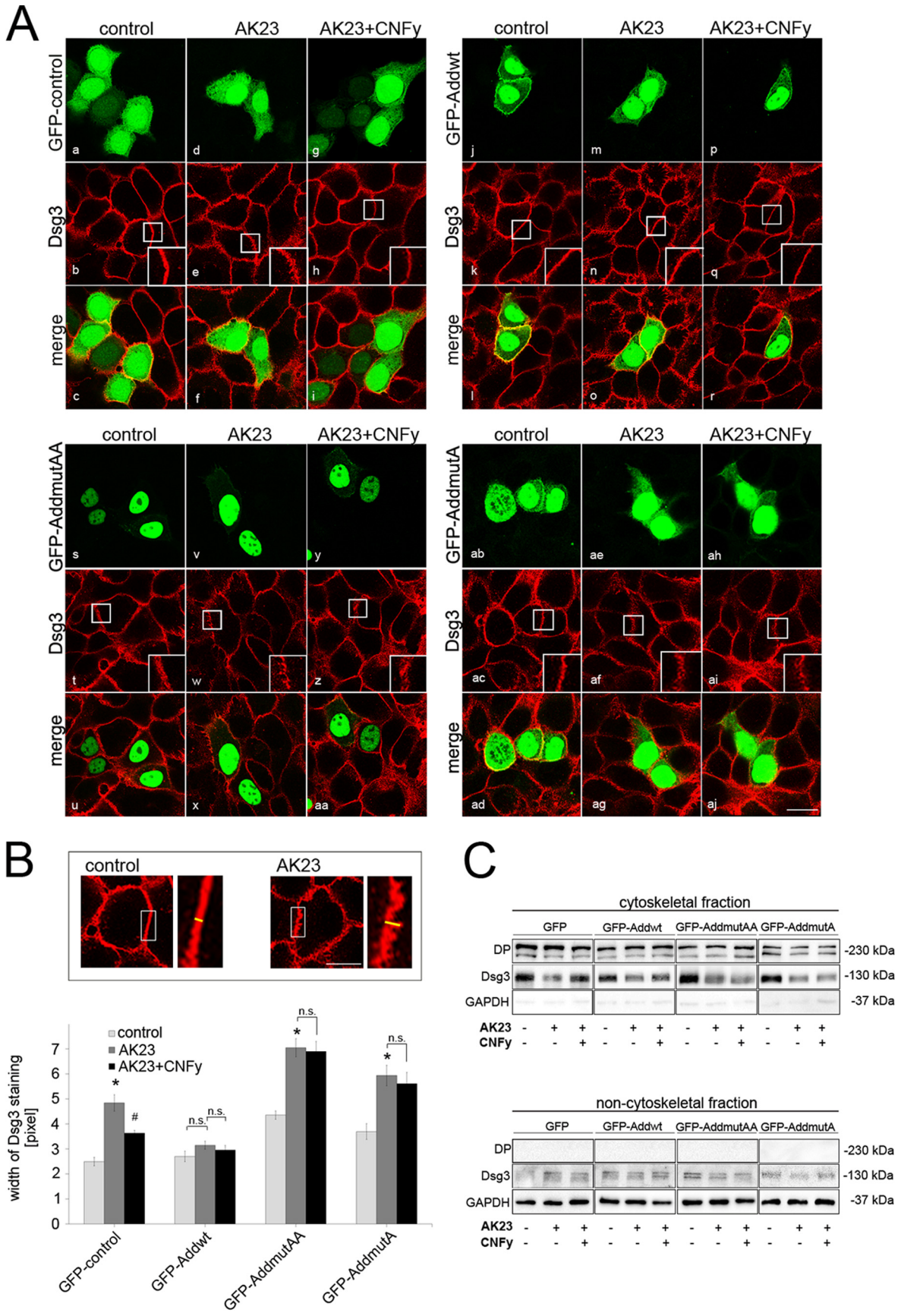
A
control
AK23
AK23+CNFy
GFP-control
GFP-Addwt
GFP-AddmutAA
GFP-AddmutA
Dsg3
merge
B
control
AK23
width of Dsg3 staining [pixel]
control
AK23
AK23+CNFy
n.s.
#
GFP-control
GFP-Addwt
GFP-AddmutAA
GFP-AddmutA
C
cytoskeletal fraction
non-cytoskeletal fraction
GFP
GFP-Addwt
GFP-AddmutAA
GFP-AddmutA
DP
Dsg3
GAPDH
-230 kDa
-130 kDa
-37 kDa
AK23
CNFy

knockdown studies, AK23-mediated cell dissociation were only partially prevented by simultaneous treatment with CNFy (GFP-AddmutAA, 43.5 ± 1.9; GFP-AddmutA, 37.75 ± 1.8 fragments). Although the results with GFP-AddmutD were similar to the other mutants and thus GFP-AddmutD had no phosphomimetic activity in this context, it still underscores the protective effect of Ser-726 phosphorylation.

To further address the role of adducin in autoantibody-mediated cell dissociation, we stained HaCaT cells expressing GFP-Addwt or GFP-Addmut after 24 h of AK23 incubation against Dsg3 (Fig. 7*A*). As previously reported for PV-IgG (17, 30) and AK23 (31, 32) in HaCaT and DJM-1 cells, AK23 treatment of control cells resulted in fragmentation of Dsg3 staining and formation of linear streaks perpendicular to the cell border (*d–f*), which led to a broadening of Dsg3 membrane staining compared with the continuously localized distribution in untreated cells (*a–c*). CNFy co-incubation prevented AK23-induced Dsg3 fragmentation (*g–i*). GFP-Addwt colocalized with Dsg3 at cell borders and was also present in the nucleus (*j–l*). Disruption of Dsg3 staining by AK23 incubation for 24 h was abolished in cells containing GFP-Addwt (*m–o*) and the parallel application of CNFy had no further effect (*p–r*). Dsg3 staining in both GFP-AddmutAA and GFP-AddmutA-transfected cells appeared weakened even under control conditions (*s–u* and *ab–ad*). Incubation with AK23 further increased fragmentation of Dsg3 staining (*v–x* and *ae–ag*), which was not prevented by CNFy co-incubation in both Addmut-transfected cells (*y–aa* and *ah–aj*). An evaluation of Dsg3 staining width at the membrane is provided in Fig. 7*B*.

Next, we investigated the effects of AK23 and CNFy on the distribution of Dsg3 in Triton X-100-soluble and -insoluble pools (Fig. 7*C*). AK23-mediated depletion of cytoskeletal Dsg3 was partially prevented by CNFy co-incubation in control cells and Addwt, but not in AddmutAA- or AddmutA-expressing cells. This is in line with the results from immunofluorescence analyses.

Taken together, these data indicate that adducin phosphorylation following pemphigus antibody incubation is independent of RhoA. However, the protective effect of exogenous RhoA activation on loss of cell adhesion relies on the presence of adducin as well as on its appropriate phosphorylation at Ser-726. Furthermore, adducin rendered phosphorylation-deficient at Ser-726 altered the regular Dsg3 distribution at the cell membrane.

PKC, but Not p38 MAPK or PKA Is Involved in PV-induced Adducin Phosphorylation—To elucidate by which pathway adducin is phosphorylated, we next focused on p38 MAPK and PKC.

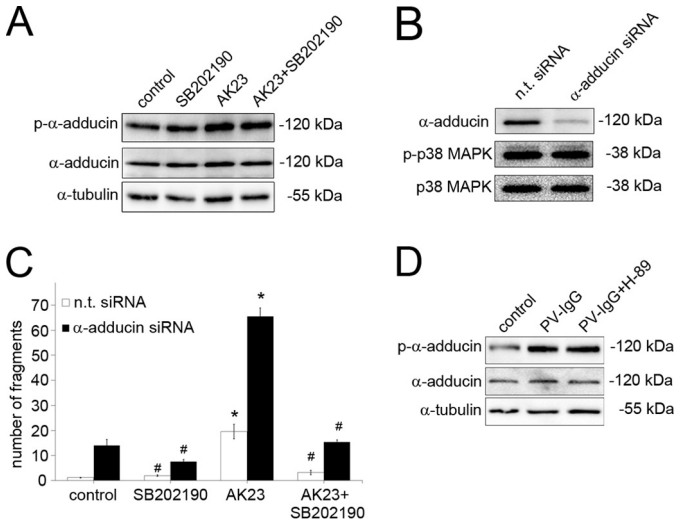

FIGURE 8. **PV-induced adducin phosphorylation is independent of p38 MAPK and PKA.** *A,* 30 min incubation with the p38 MAPK-specific inhibitor SB202190 had no effect on adducin phosphorylation compared with control. AK23 alone, but also the co-incubation with SB202190, led to increased adducin phosphorylation ($N = 4$). *B,* in Western blot analysis, alterations of p38 MAPK phosphorylation by α-adducin gene silencing were not detectable ($N = 4$). *C,* dispase-based dissociation assays showed that inhibition of p38 MAPK by SB202190 for 24 h was similarly protective in control knockdown as in α-adducin knockdown cells ($N = 8$, $n > 16$; *, $p < 0.05$ *versus* control; #, $p < 0.05$ *versus* AK23). *D,* Western blot studies demonstrated that PV-induced α-adducin phosphorylation at Ser-726 was not blocked by specific inhibition of PKA using H-89 preincubation for 2 h ($N = 3$).

The contribution of p38 MAPK to the pathogenesis of pemphigus vulgaris is well established (32, 33) and previous studies placed p38 MAPK upstream of RhoA in this context (16, 18). However, treatment of keratinocytes with the p38 MAPK inhibitor SB202190 for 30 min did not change α-adducin phosphorylation (Fig. 8*A*). Similarly, AK23-mediated adducin phosphorylation after 30 min was unaltered by p38 MAPK inhibition. Vice versa, p38 MAPK phosphorylation was unchanged following silencing of α-adducin (Fig. 8*B*). Furthermore, in dispase-based dissociation assays, inhibition of AK23-mediated cell dissociation by SB202190 was similar in control *versus* α-adducin knockdown after 24 h, as fragment numbers were reduced to the respective control levels (Fig. 8*C*). Similarly, PKA does not participate in PV-IgG-dependent adducin phosphorylation because inhibition of PKA by preincubation with H-89 did not reduce the amount of phosphorylated adducin compared with PV-IgG treatment alone (Fig. 8*D*).

Thus, we focused on PKC, which was shown to be rapidly activated following PV-autoantibody binding (34, 35) and is well known to phosphorylate adducin at Ser-726 (10). We applied the PKC inhibitor BIM-X in HaCaT cells, which pre-

FIGURE 7. **Adducin mutants enhance the effect of AK23 on Dsg3 distribution.** *A,* after transient transfection of GFP-Addwt or GFP-Addmut, cells were immunostained for Dsg3 (*red*). *Insets*, ×2 magnification of indicated areas. In cells expressing GFP only, 24 h AK23 treatment caused Dsg3 fragmentation (*d–f*) compared with controls (*a–c*). By co-incubation of CNFy, the effect induced by AK23 was abolished (*g–i*). Exogenous GFP-Addwt at cell borders (*j*) colocalized with Dsg3 staining (*k*, *l*) and abolished AK23-induced Dsg3 fragmentation (*m–o*). Parallel CNFy treatment had no further effect (*p–r*). In contrast to protective effects of GFP-Addwt expression, both GFP-AddmutAA- and GFP-AddmutA-transfected cells displayed weakened Dsg3 staining under control conditions (*s–u* and *ab–ad*) and enhanced fragmentation of Dsg3 staining by AK23 treatment (*v–x* and *ae–ag*). Under these conditions, Dsg3 fragmentation was not prevented by CNFy co-treatment (*y–aa* and *ah–aj*). *Scale bar*: 20 μm ($N = 4$). *B*, width of Dsg3 staining was quantified with ImageJ as depicted in the *upper panel*. Dsg3 width at the membrane (*yellow dashes*, *insets*, ×3 magnification of areas indicated) was determined at four sides of each transfected cell after respective treatment. Cells were imaged at strictly the same magnification and settings. *Scale bar*, 20 μm. *Lower panel* shows the result of image analysis ($N = 4$, $N > 16$ cells per condition; *, $p < 0.05$ *versus* control; #, $p < 0.05$ *versus* AK23). *C,* immunoblot analysis following Triton X-100-mediated cell fractionation revealed that AK23-induced depletion of the cytoskeleton-bound fraction of Dsg3 was partially blocked by CNFy co-incubation in control cells and GFP-Addwt, but not in GFP-AddmutAA- or GFP-AddmutA-transfected cells ($N = 4$).

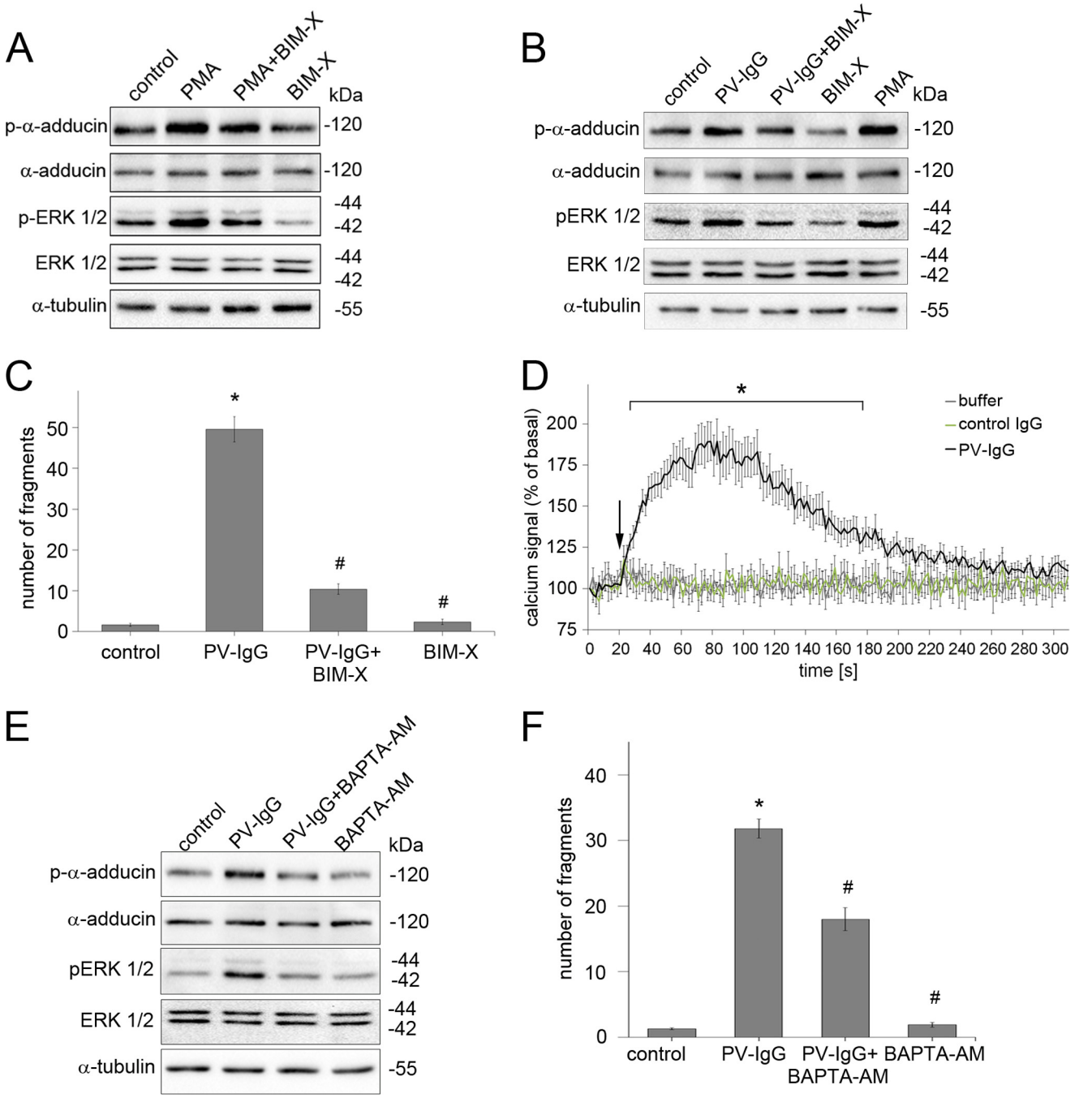

FIGURE 9. **Adducin phosphorylation in response to PV-IgG is mediated via Ca^{2+}-dependent PKC signaling.** *A*, in immunoblot analysis, phosphorylation of adducin by incubation of the specific PKC activator PMA for 10 min was blocked by co-incubation of PKC inhibitor BIM-X. The effectiveness of PKC modulators was tested by ERK phosphorylation analyses ($N = 4$). *B*, PV-IgG-induced adducin phosphorylation after 10 min was abolished by co-treatment with BIM-X. *C*, similarly, simultaneous incubation with BIM-X prevented cell dissociation induced by 24 h PV-IgG incubation ($N = 5$, $n > 10$; *, $p < 0.05$ *versus* control; #, $p < 0.05$ *versus* PV-IgG). *D*, in aequorin-based Ca^{2+}-measuring assays, a PV-IgG-specific rapid increase of cytosolic Ca^{2+} levels was detectable. *E*, Western blot analysis revealed that BAPTA-AM incubation for 4 h blocked both the PV-IgG-induced adducin phosphorylation as well as ERK-phosphorylation ($N = 3$). *F*, BAPTA-AM co-incubation for 4 h prevented loss of cell adhesion caused by PV-IgG ($N = 4$, $n > 8$; *, $p < 0.05$ *versus* control; #, $p < 0.05$ PV-IgG).

vented adducin phosphorylation induced by the PKC activator PMA as well as phosphorylation of extracellular signal-regulated kinases-1/2 (ERK1/2), another well established PKC target (36) (Fig. 9*A*). PV-IgG-mediated phosphorylation of adducin after 10 min was abolished by simultaneous PKC inhibition via BIM-X (Fig. 9*B*). Furthermore, simultaneous incubation with BIM-X prevented cell dissociation induced by 24 h PV-IgG incubation (10.4 ± 1.3 *versus* 49.6 ± 3.1 fragments; Fig. 9*C*). Conventional PKC isoforms require Ca^{2+} for activation (37) and it has previously been shown that PV-IgG induce a rapid increase in cytosolic Ca^{2+} levels (38). Similar in our study, a PV-IgG-specific increase in cytosolic Ca^{2+} was detectable by aequorin-based calcium assays (28) starting immediately after injection of autoantibodies and lasting ~180 s (Fig. 9*D*). Most importantly, preincubation with the cell-permeable Ca^{2+}-chelating agent BAPTA-AM prevented both adducin and ERK

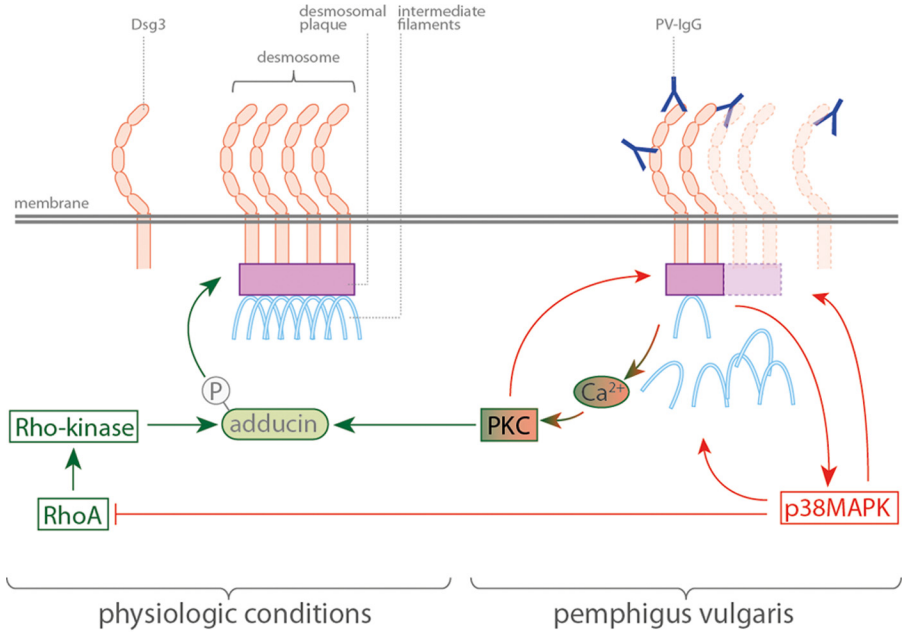

FIGURE 10. **Summary of adducin signaling to desmosomes.** *Green lines and arrows* symbolize adhesion-enhancing signaling, *red lines and arrows* denote signaling provoking loss of cell cohesion. Under physiologic conditions, adducin promotes Dsg3 incorporation into desmosomes. In this regard, RhoA signaling via Rho kinase may be required for adducin phosphorylation at Ser-726. Under conditions of PV-IgG incubation, both PKC and p38 MAPK are activated. Active p38 MAPK reduces RhoA activity and thereby disrupts RhoA-mediated desmosome assembly, which promotes Dsg3 depletion. PKC exhibits a dual function on cell cohesion: on one hand it promotes cell dissociation, which thus is similar to the function of p38 MAPK. On the other hand, PKC enhances keratinocyte cohesion via phosphorylation of adducin. However, this may be ineffective to block the effects of p38 MAPK. Nevertheless, exogenous activation of RhoA promotes the desmosome assembly pathway, which is then capable of preventing PV-IgG-induced cell cohesion loss.

phosphorylation, the latter indicative of PKC activation (Fig. 9*E*). Similar to PKC inhibition, BAPTA-AM co-treatment prevented cell dissociation induced by 4 h of PV-IgG incubation (18.0 ± 1.7 *versus* 31.8 ± 1.5 fragments; Fig. 9*F*). Collectively, our data indicate that adducin phosphorylation in response to pemphigus autoantibodies is mediated via Ca^{2+}-dependent PKC signaling.

DISCUSSION

Adducin Regulates Keratinocyte Cell-Cell Cohesion—Although regulation of the membrane cytoskeleton by adducin is well established (3, 4) and previous studies demonstrated association of adducin with intercellular contacts (7, 8), there is little insight into the functional role of adducin for intercellular adhesion. Here we show that adducin is indispensable for keratinocyte cohesion, which is in line with a study suggesting that depletion of α-adducin impairs E-cadherin-mediated adhesion of MDCK cells (39). In our study we demonstrate that specific α- or γ-adducin knockdown resulted in loss of keratinocyte cohesion and in reduction of Dsg3 protein content in the cytoskeleton-bound pool, interestingly without affecting E-cadherin. These data suggest that adducin controls keratinocyte cohesion specifically by regulating desmosomal Dsg3 levels. Previously, a direct interaction of Dsg3 and actin was demonstrated, however, in the non-cytoskeletal pool only and not in Dsg3 connected to the cytoskeleton (24). Nevertheless, a direct regulation of Dsg3 by adducin, *i.e.* as a scaffolding protein, is unlikely because we did not observe an interaction of adducin and Dsg3 in immunoprecipitation experiments (data not shown). Thus, it is likely that adducin modulates Dsg3 turnover via its influence on the cortical actin cytoskeleton (20).

An indirect regulation of Dsg3 levels by adducin is conceivable by modulating its turnover in desmosomes. Indeed, it has been shown that desmoplakin is transported to the membrane via an actin-driven mechanism on establishment of cell-cell contact (40), a process that may require plakophilin-2 and RhoA (41). Our data from FRAP experiments indicate that primarily the assembly pathway of Dsg3 to the desmosome is modulated by adducin. In this context, adducin may be involved in regulating the lateral incorporation of Dsg3 into desmosomes. Newly synthesized Dsg3 was shown to first be transported to the membrane and subsequently becoming incorporated into already existing desmosomes (42). The cortical actin cytoskeleton restricts lateral mobility and shapes clusters of membrane proteins by forming a net-like structure, with the actin filaments building the fences (43–45). Adducin may serve to control this "corralling" function of the actin membrane cytoskeleton and thereby regulate lateral shifts of Dsg3 into desmosomes. It has been shown that PKC-mediated adducin phosphorylation at Ser-726 reduced actin binding and induced its redistribution away from the cell membrane (6). In line with this, we observed fragmentation of adducin staining at sites where PV-IgG caused intercellular gap formation. Thus, redistribution of adducin at sites where cell junctions are disrupted or reduced binding of adducin to actin may alter cortical actin dynamics that are required to promote Dsg3 incorporation into desmosomes. Up to now it is unclear why adducin affects Dsg3 levels but not the levels of E-cadherin. It is possible that the mechanisms by which desmosomal cadherins are targeted to the cell membrane are different compared with E-cadherin, or that the sorting of the adhesion molecules into their respective

junctional compartment requires distinct contributions of the actin cytoskeleton (46). The latter is supported by the recent finding that the assembly of desmosomes but not of adherens junctions is lipid raft-dependent (47). Further work is not only required to elucidate these aspects but also needs to investigate whether adducin regulation is restricted to Dsg3 or affects other desmosmal adhesion molecules as well.

Adducin Phosphorylation by PKC May Represent a Protective Mechanism in Response to Pemphigus Autoantibodies Which Is Augmented by RhoA—One unexpected observation was that both pemphigus autoantibodies (destabilizing cell adhesion) and RhoA activation (stabilizing cell adhesion) induced phosphorylation of adducin. We interpret these results that binding of pemphigus autoantibodies induces protective signaling within keratinocytes (Fig. 10, *green arrows*). This is underscored by the fact that the effect of AK23 was pronounced after introduction of the phosphorylation-deficient mutant of α-adducin. The concept of rescue mechanisms triggered by autoantibody binding is conceivable because it was previously shown that keratinocytes increase the amount of cAMP to reduce cell dissociation (48). Our data demonstrate that phosphorylation of adducin at Ser-726 is mediated, either directly or indirectly, by PKC. Furthermore, PKC activation in response to pemphigus autoantibodies is likely Ca^{2+}-dependent. This is in line with previous studies implicating Ca^{2+}/PKC signaling in pemphigus (38, 49, 50). Based on the fact that conventional PKC isoforms require Ca^{2+}, it may be concluded that adducin phosphorylation in this context relies on these classical PKC isoforms. Our data demonstrate that PKC activation in response to autoantibody treatment results both in adhesion-protective signaling such as adducin phosphorylation as well as in cell dissociation (Fig. 10, *red arrows*). This is shown by our experiments in which both PKC inhibition as well as inhibition of Ca^{2+} signaling prevented cell dissociation after pemphigus autoantibody binding. Thus, the effect of PKC activation in response to pemphigus autoantibodies is complex (20, 51) (Fig. 10). Indeed, the dual function of PKC to promote and destabilize desmosomal adhesion is well recognized in the literature (52). For destabilization, PKC appears to render Dsg3 susceptible for autoantibody-induced depletion (34, 53) and prevent hyperadhesion (54), possibly by phosphorylation of desmoplakin (55, 56). For stabilization, plakophilin-2 was shown to recruit PKC to promote desmosome formation and keratin filament anchorage (57). At present it is unclear how the balance of stabilizing and destabilizing mechanisms in response to autoantibody binding is tuned.

RhoA probably is not involved in the phosphorylation of adducin in response to autoantibody treatment because RhoA activity was reduced at time points when adducin was phosphorylated. Nevertheless, pharmacological activation of RhoA by CNFy may enhance this protective pathway of adducin phosphorylation (Fig. 10). The present study extends our previous observations on the protective effect of RhoA-mediated actin modulation in pemphigus and identifies phosphorylation of adducin at Ser-726, possibly via Rho-kinase, to be important for strengthening cell adhesion. The fact that the protective effect of RhoA activation was only partially inhibited under conditions of adducin knockdown may be explained by the remaining adducin that was not targeted by siRNA. In addition, our previous findings demonstrated that activation of RhoA also prevents keratin retraction, a hallmark of pemphigus (16). In this study, p38 MAPK reduced RhoA signaling following PV-IgG incubation, which also would be expected to result in reduced adducin phosphorylation. This may, however, be masked by simultaneous PKC activation.

It is unclear whether PKC and Rho-kinase both directly phosphorylate adducin at Ser-726. This residue was initially shown to be phosphorylated by PKC and PKA (1, 10). Thus, it is possible that Rho-kinase acts upstream of PKC. The precise mechanisms of Ser-726 phosphorylation need to be determined in future studies.

Acknowledgments—We are grateful to Dr. Hong-Chen Chen and Dr. Yasushi Hanakawa for providing the adducin and Dsg3 constructs. We thank Dr. Kathleen Green for donating an antibody and Dr. Enno Schmidt for supporting us with pemphigus sera. Furthermore, we thank Angelika Antonius, Martina Hitzenbichler, Sabine Muehlsimer, and Andrea Wehmeyer for skillful technical assistance, and Dr. Angela Schlipp, Dr. Mariya Radeva, and Eva Hartlieb for helpful scientific discussions.

REFERENCES

1. Matsuoka, Y., Li, X., and Bennett, V. (2000) Adducin: structure, function and regulation. *Cell. Mol. Life Sci.* **57,** 884–895
2. Hughes, C. A., and Bennett, V. (1995) Adducin: a physical model with implications for function in assembly of spectrin-actin complexes. *J. Biol. Chem.* **270,** 18990–18996
3. Li, X., Matsuoka, Y., and Bennett, V. (1998) Adducin preferentially recruits spectrin to the fast growing ends of actin filaments in a complex requiring the MARCKS-related domain and a newly defined oligomerization domain. *J. Biol. Chem.* **273,** 19329–19338
4. Kuhlman, P. A., Hughes, C. A., Bennett, V., and Fowler, V. M. (1996) A new function for adducin: calcium/calmodulin-regulated capping of the barbed ends of actin filaments. *J. Biol. Chem.* **271,** 7986–7991
5. Taylor, K. A., and Taylor, D. W. (1994) Formation of two-dimensional complexes of F-actin and crosslinking proteins on lipid monolayers: demonstration of unipolar α-actinin-F-actin cross-linking. *Biophys. J.* **67,** 1976–1983
6. Kaiser, H. W., O'Keefe, E., and Bennett, V. (1989) Adducin: Ca^{2+}-dependent association with sites of cell-cell contact. *J. Cell Biol.* **109,** 557–569
7. Dong, L., Chapline, C., Mousseau, B., Fowler, L., Ramsay, K., Stevens, J. L., and Jaken, S. (1995) 35H, a sequence isolated as a protein kinase C-binding protein, is a novel member of the adducin family. *J. Biol. Chem.* **270,** 25534–25540
8. Naydenov, N. G., and Ivanov, A. I. (2010) Adducins regulate remodeling of apical junctions in human epithelial cells. *Mol. Biol. Cell* **21,** 3506–3517
9. Gardner, K., and Bennett, V. (1987) Modulation of spectrin-actin assembly by erythrocyte adducin. *Nature* **328,** 359–362
10. Matsuoka, Y., Hughes, C. A., and Bennett, V. (1996) Adducin regulation. Definition of the calmodulin-binding domain and sites of phosphorylation by protein kinases A and C. *J. Biol. Chem.* **271,** 25157–25166
11. Fukata, Y., Oshiro, N., Kinoshita, N., Kawano, Y., Matsuoka, Y., Bennett, V., Matsuura, Y., and Kaibuchi, K. (1999) Phosphorylation of adducin by Rho-kinase plays a crucial role in cell motility. *J. Cell Biol.* **145,** 347–361
12. Kimura, K., Fukata, Y., Matsuoka, Y., Bennett, V., Matsuura, Y., Okawa, K., Iwamatsu, A., and Kaibuchi, K. (1998) Regulation of the association of adducin with actin filaments by Rho-associated kinase (Rho-kinase) and myosin phosphatase. *J. Biol. Chem.* **273,** 5542–5548
13. Maekawa, M., Ishizaki, T., Boku, S., Watanabe, N., Fujita, A., Iwamatsu, A., Obinata, T., Ohashi, K., Mizuno, K., and Narumiya, S. (1999) Signaling

from Rho to the actin cytoskeleton through protein kinases ROCK and LIM-kinase. *Science* **285,** 895–898
14. Amano, M., Mukai, H., Ono, Y., Chihara, K., Matsui, T., Hamajima, Y., Okawa, K., Iwamatsu, A., and Kaibuchi, K. (1996) Identification of a putative target for Rho as the serine-threonine kinase protein kinase N. *Science* **271,** 648–650
15. Hall, A. (1998) Rho GTPases and the actin cytoskeleton. *Science* **279,** 509–514
16. Waschke, J., Spindler, V., Bruggeman, P., Zillikens, D., Schmidt, G., and Drenckhahn, D. (2006) Inhibition of RhoA activity causes pemphigus skin blistering. *J. Cell Biol.* **175,** 721–727
17. Spindler, V., Drenckhahn, D., Zillikens, D., and Waschke, J. (2007) Pemphigus IgG causes skin splitting in the presence of both desmoglein 1 and desmoglein 3. *Am. J. Pathol.* **171,** 906–916
18. Spindler, V., and Waschke, J. (2011) Role of Rho GTPases in desmosomal adhesion and pemphigus pathogenesis. *Ann. Anat.* **193,** 177–180
19. Amagai, M., and Stanley, J. R. (2012) Desmoglein as a target in skin disease and beyond. *J. Invest. Dermatol.* **132,** 776–784
20. Waschke, J., and Spindler, V. (2014) Desmosomes and extradesmosomal adhesive signaling contacts in pemphigus. *Med. Res. Rev.* 10.1002/med.21310
21. Berkowitz, P., Hu, P., Liu, Z., Diaz, L. A., Enghild, J. J., Chua, M. P., and Rubenstein, D. S. (2005) Desmosome signaling. Inhibition of p38MAPK prevents pemphigus vulgaris IgG-induced cytoskeleton reorganization. *J. Biol. Chem.* **280,** 23778–23784
22. Waschke, J., Bruggeman, P., Baumgartner, W., Zillikens, D., and Drenckhahn, D. (2005) Pemphigus foliaceus IgG causes dissociation of desmoglein 1-containing junctions without blocking desmoglein 1 transinteraction. *J. Clin. Invest.* **115,** 3157–3165
23. Gliem, M., Heupel, W. M., Spindler, V., Harms, G. S., and Waschke, J. (2010) Actin reorganization contributes to loss of cell adhesion in pemphigus vulgaris. *Am. J. Physiol. Cell Physiol.* **299,** C606–613
24. Tsang, S. M., Brown, L., Gadmor, H., Gammon, L., Fortune, F., Wheeler, A., and Wan, H. (2012) Desmoglein 3 acting as an upstream regulator of Rho GTPases, Rac-1/Cdc42 in the regulation of actin organisation and dynamics. *Exp. Cell Res.* **318,** 2269–2283
25. Tsunoda, K., Ota, T., Aoki, M., Yamada, T., Nagai, T., Nakagawa, T., Koyasu, S., Nishikawa, T., and Amagai, M. (2003) Induction of pemphigus phenotype by a mouse monoclonal antibody against the amino-terminal adhesive interface of desmoglein 3. *J. Immunol.* **170,** 2170–2178
26. Chen, C. L., Hsieh, Y. T., and Chen, H. C. (2007) Phosphorylation of adducin by protein kinase Cδ promotes cell motility. *J. Cell Sci.* **120,** 1157–1167
27. Hartlieb, E., Kempf, B., Partilla, M., Vigh, B., Spindler, V., and Waschke, J. (2013) Desmoglein 2 is less important than desmoglein 3 for keratinocyte cohesion. *PLoS One* **8,** e53739
28. Baubet, V., Le Mouellic, H., Campbell, A. K., Lucas-Meunier, E., Fossier, P., and Brúlet, P. (2000) Chimeric green fluorescent protein-aequorin as bioluminescent Ca^{2+} reporters at the single-cell level. *Proc. Natl. Acad. Sci. U.S.A.* **97,** 7260–7265
29. Sato, M., Aoyama, Y., and Kitajima, Y. (2000) Assembly pathway of desmoglein 3 to desmosomes and its perturbation by pemphigus vulgaris-IgG in cultured keratinocytes, as revealed by time-lapsed labeling immunoelectron microscopy. *Lab. Invest.* **80,** 1583–1592
30. Heupel, W. M., Zillikens, D., Drenckhahn, D., and Waschke, J. (2008) Pemphigus vulgaris IgG directly inhibit desmoglein 3-mediated transinteraction. *J. Immunol.* **181,** 1825–1834
31. Yamamoto, Y., Aoyama, Y., Shu, E., Tsunoda, K., Amagai, M., and Kitajima, Y. (2007) Anti-desmoglein 3 (Dsg3) monoclonal antibodies deplete desmosomes of Dsg3 and differ in their Dsg3-depleting activities related to pathogenicity. *J. Biol. Chem.* **282,** 17866–17876
32. Spindler, V., Rötzer, V., Dehner, C., Kempf, B., Gliem, M., Radeva, M., Hartlieb, E., Harms, G. S., Schmidt, E., and Waschke, J. (2013) Peptide-mediated desmoglein 3 crosslinking prevents pemphigus vulgaris autoantibody-induced skin blistering. *J. Clin. Invest.* **123,** 800–811
33. Evans, J. V., Ammer, A. G., Jett, J. E., Bolcato, C. A., Breaux, J. C., Martin, K. H., Culp, M. V., Gannett, P. M., and Weed, S. A. (2012) Src binds cortactin through an SH2 domain cystine-mediated linkage. *J. Cell Sci.* **125,** 6185–6197
34. Spindler, V., Endlich, A., Hartlieb, E., Vielmuth, F., Schmidt, E., and Waschke, J. (2011) The extent of desmoglein 3 depletion in pemphigus vulgaris is dependent on Ca^{2+}-induced differentiation: a role in suprabasal epidermal skin splitting? *Am. J. Pathol.* **179,** 1905–1916
35. Head, J. A., Jiang, D., Li, M., Zorn, L. J., Schaefer, E. M., Parsons, J. T., and Weed, S. A. (2003) Cortactin tyrosine phosphorylation requires Rac1 activity and association with the cortical actin cytoskeleton. *Mol. Biol. Cell* **14,** 3216–3229
36. Schönwasser, D. C., Marais, R. M., Marshall, C. J., and Parker, P. J. (1998) Activation of the mitogen-activated protein kinase/extracellular signal-regulated kinase pathway by conventional, novel, and atypical protein kinase C isotypes. *Mol. Cell. Biol.* **18,** 790–798
37. Mochly-Rosen, D., Das, K., and Grimes, K. V. (2012) Protein kinase C, an elusive therapeutic target? *Nat. Rev. Drug Discov.* **11,** 937–957
38. Seishima, M., Esaki, C., Osada, K., Mori, S., Hashimoto, T., and Kitajima, Y. (1995) Pemphigus IgG, but not bullous pemphigoid IgG, causes a transient increase in intracellular calcium and inositol 1,4,5-triphosphate in DJM-1 cells, a squamous cell carcinoma line. *J. Invest. Dermatol.* **104,** 33–37
39. Chen, C. L., Lin, Y. P., Lai, Y. C., and Chen, H. C. (2011) α-Adducin translocates to the nucleus upon loss of cell-cell adhesions. *Traffic* **12,** 1327–1340
40. Okamura, H., and Resh, M. D. (1995) p80/85 cortactin associates with the Src SH2 domain and colocalizes with v-Src in transformed cells. *J. Biol. Chem.* **270,** 26613–26618
41. Nieto-Pelegrin, E., and Martinez-Quiles, N. (2009) Distinct phosphorylation requirements regulate cortactin activation by TirEPEC and its binding to N-WASP. *Cell Commun. Signal.* **7,** 11
42. Kirkbride, K. C., Hong, N. H., French, C. L., Clark, E. S., Jerome, W. G., and Weaver, A. M. (2012) Regulation of late endosomal/lysosomal maturation and trafficking by cortactin affects Golgi morphology. *Cytoskeleton* **69,** 625–643
43. Kusumi, A., Suzuki, K., and Koyasako, K. (1999) Mobility and cytoskeletal interactions of cell adhesion receptors. *Curr. Opin. Cell Biol.* **11,** 582–590
44. Sako, Y., Nagafuchi, A., Tsukita, S., Takeichi, M., and Kusumi, A. (1998) Cytoplasmic regulation of the movement of E-cadherin on the free cell surface as studied by optical tweezers and single particle tracking: corralling and tethering by the membrane skeleton. *J. Cell Biol.* **140,** 1227–1240
45. Baumgartner, W., Schütz, G. J., Wiegand, J., Golenhofen, N., and Drenckhahn, D. (2003) Cadherin function probed by laser tweezer and single molecule fluorescence in vascular endothelial cells. *J. Cell Sci.* **116,** 1001–1011
46. Green, K. J., Getsios, S., Troyanovsky, S., and Godsel, L. M. (2010) Intercellular junction assembly, dynamics, and homeostasis. *Cold Spring Harbor Perspect. Biol.* **2,** a000125
47. Stahley, S. N., Saito, M., Faundez, V., Koval, M., Mattheyses, A. L., and Kowalczyk, A. P. (2014) Desmosome assembly and disassembly are membrane raft-dependent. *PLoS One* **9,** e87809
48. Spindler, V., Vielmuth, F., Schmidt, E., Rubenstein, D. S., and Waschke, J. (2010) Protective endogenous cyclic adenosine 5′-monophosphate signaling triggered by pemphigus autoantibodies. *J. Immunol.* **185,** 6831–6838
49. Esaki, C., Seishima, M., Yamada, T., Osada, K., and Kitajima, Y. (1995) Pharmacologic evidence for involvement of phospholipase C in pemphigus IgG-induced inositol 1,4,5-trisphosphate generation, intracellular calcium increase, and plasminogen activator secretion in DJM-1 cells, a squamous cell carcinoma line. *J. Invest. Dermatol.* **105,** 329–333
50. Osada, K., Seishima, M., and Kitajima, Y. (1997) Pemphigus IgG activates and translocates protein kinase C from the cytosol to the particulate/cytoskeleton fractions in human keratinocytes. *J. Invest. Dermatol.* **108,** 482–487
51. Spindler, V., and Waschke, J. (2014) Desmosomal cadherins and signaling: lessons from autoimmune disease. *Cell. Commun. Adhes.* **21,** 77–84
52. Waschke, J. (2008) The desmosome and pemphigus. *Histochem. Cell Biol.* **130,** 21–54
53. Cirillo, N., Lanza, A., and Prime, S. S. (2010) Induction of hyper-adhesion attenuates autoimmune-induced keratinocyte cell-cell detachment and

processing of adhesion molecules via mechanisms that involve PKC. *Exp. Cell Res.* **316,** 580–592
54. Kimura, T. E., Merritt, A. J., and Garrod, D. R. (2007) Calcium-independent desmosomes of keratinocytes are hyper-adhesive. *J. Invest. Dermatol.* **127,** 775–781
55. Hobbs, R. P., and Green, K. J. (2012) Desmoplakin regulates desmosome hyperadhesion. *J. Invest. Dermatol.* **132,** 482–485
56. Kröger, C., Loschke, F., Schwarz, N., Windoffer, R., Leube, R. E., and Magin, T. M. (2013) Keratins control intercellular adhesion involving PKC-α-mediated desmoplakin phosphorylation. *J. Cell Biol.* **201,** 681–692
57. Bass-Zubek, A. E., Hobbs, R. P., Amargo, E. V., Garcia, N. J., Hsieh, S. N., Chen, X., Wahl, J. K., 3rd, Denning, M. F., and Green, K. J. (2008) Plakophilin 2: a critical scaffold for PKCα that regulates intercellular junction assembly. *J. Cell Biol.* **181,** 605–613